



# Accelerated degradation of Pt<sub>3</sub>Co/C and Pt/C electrocatalysts studied by identical-location transmission electron microscopy in polymer electrolyte environment



Flávio R. Nikkuni<sup>a,b,c,1</sup>, Laetitia Dubau<sup>a,b</sup>, Edson A. Ticianelli<sup>c</sup>, Marian Chatenet<sup>a,b,d,\*</sup>

<sup>a</sup> Univ Grenoble Alpes, LEPMI, F-38000 Grenoble, France

<sup>b</sup> CNRS, LEPMI, F-38000 Grenoble, France

<sup>c</sup> Instituto de Química de São Carlos, Univ. de São Paulo, Avenida Trabalhador São-carlense, 400 Parque Arnold Schmidt, CP 780, 13560-970 São Carlos, SP, Brazil

<sup>d</sup> Institut Universitaire de France (IUF), Paris, France

## ARTICLE INFO

### Article history:

Received 30 January 2015

Received in revised form 9 April 2015

Accepted 16 April 2015

Available online 17 April 2015

### Keywords:

Identical location transmission electron microscopy (IL-TEM)  
UltraMicroElectrode with cavity (UMEC)  
Oxygen reduction reaction (ORR)  
Platinum–cobalt nanostructured electrocatalysts degradation  
Proton exchange membrane fuel cell (PEMFC)

## ABSTRACT

Identical-location transmission electron microscopy (ILTEM) coupled with X-ray energy dispersive spectroscopy (X-EDS) analyses were used to characterize the changes in the morphology and composition of Pt and Pt<sub>3</sub>Co nanoparticles deposited on high surface area carbon (Vulcan XC72) before and after electrochemical ageing tests performed in polymer electrolyte environment, using a “dry cell”. The Pt/C and Pt<sub>3</sub>Co/C electrocatalysts are modified upon electrochemical ageing, following changes in particle size, geometry, and composition; these changes are however milder to what happens upon aging in H<sub>2</sub>SO<sub>4</sub> electrolyte, because of the lack of liquid water, a reactant in both carbon corrosion and Pt (Pt<sub>3</sub>Co) corrosion/dissolution reactions. The negative vertex potential of the ageing procedure also matters: Pt redeposition occurs at 0.1 V vs. RHE and not at 0.6 V vs. RHE, while carbon corrosion is emphasized after incursions at the lower vertex potential, in agreement to what demonstrated in liquid electrolyte. Besides, the presence of Co in Pt<sub>3</sub>Co alloys enables to somewhat slow-down the Pt corrosion from Pt<sub>3</sub>Co/C electrocatalysts, since cobalt acts as a sacrificial anode, which also lowers carbon corrosion.

These morphology and composition changes were further used to explain the changes in ORR intrinsic activity of the electrocatalysts upon electrochemical aging; the ORR activity and the accelerated stress tests (AST) were measured/performed in a similar setup (at the interface with a polymer electrolyte) using an ultramicroelectrode with cavity. The ORR activity only improved for Pt/C nanoparticles when the AST contained the lower vertex potential (0.1 V vs. RHE), thanks to the favorable increase of the particle sizes, favored because the Pt<sup>2+</sup> ions released by the corrosion of the Pt/C nanoparticles at 0.9 V vs. RHE remains trapped in the Nafion®, thereby easing its redeposition in the subsequent step at 0.1 V vs. RHE. In all the other cases, the ORR activity decreased upon the AST. On Pt<sub>3</sub>Co/C the positive effect of Pt redeposition in the 0.1–0.9 V vs. RHE ageing procedure is counterbalanced by a detrimental (and large) effect of Co dissolution, which adversely affects the nanoparticles composition for the ORR and pollutes the polymer electrolyte membrane (the Co<sup>3+</sup> cations hinder O<sub>2</sub> and H<sup>+</sup> transport in the electrolyte membrane). After the 0.6–0.9 V vs. RHE ageing procedure, the ORR activity always decreases, because the redeposition of Pt is not likely, therefore suppressing the positive effect of particle size increase monitored in the 0.1–0.9 V vs. RHE ageing procedure, and because Co dissolution and adverse effect is maintained.

© 2015 Elsevier B.V. All rights reserved.

## 1. Introduction

The unavoidable development of green energy production and storage calls for devices that can efficiently and durably convert electricity into chemical energy and vice versa [1]. In that frame, building fleets of water electrolyzers that produce clean hydrogen, H<sub>2</sub> (and oxygen, O<sub>2</sub>) and fuel cells that convert this H<sub>2</sub> into electricity (using the oxygen from air) is a practically viable

\* Corresponding author at: CNRS, LEPMI, F-38000 Grenoble, France.  
Tel.: +33 476 826 588; fax: +33 476 826 777.

E-mail address: [Marian.Chatenet@grenoble-inp.fr](mailto:Marian.Chatenet@grenoble-inp.fr) (M. Chatenet).

<sup>1</sup> Present address: Fundação Parque Tecnológico Itaipu – Projeto baterias, Av. Tancredo Neves, 6731, Caixa Postal 2039, CEP 85.867-900, Foz do Iguaçu – Paraná, Brazil.

technology; numerous demonstrators bloom on the planet, in stationary, (auto) mobile and portable applications, with their number increasing at an exponential pace since the 2010s. Today, the most technologically-advanced and performant fuel cell systems are based on proton-conducting membranes of the perfluorosulfonic family (proton exchange membrane fuel cells, PEMFCs) [2,3] and proton exchange membrane electrolysis cells (PEMECs) are viewed as a possible alternatives to the present alkaline electrolysis cells [4]. Both systems rely on electrocatalytic reactions, and in any case, it is the oxygen-related reaction that limits the system performances. For example in a PEMFC, catalyzing the sluggish oxygen reduction reaction (ORR) in more efficient and durable manners has been one of the major scientific endeavor of the past decades [2,3].

Although platinum (Pt), used as nanocrystallites deposited on high surface area carbon (Pt/C) to optimize the performance-to-metal cost ratio, is the best ORR electrocatalysts in acidic medium, its activity and durability is not sufficient in PEMFC conditions [2,5–8]. Both parameters can supposedly be improved by alloying platinum with less noble metal, usually of the transition metal family (PtM/C, e.g., with M = Co, Ni or Cu), and the literature contains numerous examples of such PEMFC cathodes electrocatalyst [7,9–12]. It has to be noted that the activity of PtM/C electrocatalysts depends on their structure, morphology, composition and particle size [11–17], and that all these features undergo severe modification upon PEMFC operation [18–20]. Therefore, elucidating how these materials degrade was a hot topic of the last decade. Some studies dealt with real PEMFC tests (usually of PEMFC stacks or PEMFC single cells operated for several 1000 h on the field, or at least in “real” conditions of use) [5,6,18,19,21–30] while others consisted in accelerated stress tests (AST), usually performed in three-electrode cells in liquid electrolyte conditions [31–38].

Unfortunately, the conclusions derived from the two types of test are not always in agreement. Among other explanations, it is quite obvious that an AST performed in aqueous electrolyte solution can yield degradation mechanisms and kinetics that differ from what happens in a real PEMFC, because water participates to the degradation mechanisms of PtM/C electrocatalysts [39,40]. This clearly puts into question the relevance of such AST in liquid electrolyte solutions to mimic (in an accelerate manner) real PEMFC degradations.

To unveil this blur, this paper explores the role played by liquid water, in the degradation mechanisms of PtM/C electrocatalysts. For that purpose, two state-of-the-art commercial electrocatalysts have been investigated and considered as benchmark materials: Pt/C and Pt<sub>3</sub>Co/C, both loaded at 20 wt% of metal over Vulcan XC72 high-surface-area carbon substrate from E-Tek. AST were performed on these materials, using a “dry cell” that uses a Nafion® 115 membrane as the electrolyte (see Supplementary Fig. S1 in [41]). Two types of working electrodes were employed. On the one hand, the PtM/C electrocatalyst was immobilized onto a gold TEM grid to monitor the structural and chemical changes of identical alloy nanoparticles prior/after the AST using Identical Location Transmission Electron Microscopy (IL-TEM), a technique developed by Mayrhofer et al. and mostly used in liquid electrolyte so far [37,42–45]. Our previous contribution [41] however demonstrated that the technique was exploitable for polymer-electrolytes as well, the study having started to unveil the role played by water in the degradation of Pt<sub>3</sub>Co/C electrocatalysts upon an AST performed between 0.1 and 0.9 V vs. RHE.

In the present paper, we further extend the study to another AST (between 0.6 and 0.9 V vs. RHE) and to pure platinum electrocatalysts (Pt/C), to probe the influence of the lower vertex potential of the AST and of the composition of the electrocatalyst on the mechanisms and extent of degradation. On the other hand, using an ultramicroelectrode with cavity (UMEC) filled with Pt/C or Pt<sub>3</sub>Co/C

nanoparticles as the working electrode in the dry cell (conditions that enable to mimic those of a PEMFC, at least for the electrocatalyst operation [27,41,46]), the intrinsic ORR kinetics of each electrocatalyst at the interface with Nafion® was determined, and its relative changes after vs. before each AST were determined. The experiments were compared with similar ones performed in liquid electrolyte (same electrocatalyst, potential variations and test durations) [31] and in a single PEMFC.

## 2. Experimental

### 2.1. Materials and electrochemical devices and procedures

The two commercial electrocatalysts investigated in the present study are: Pt/C and Pt<sub>3</sub>Co/C from E-Tek; the metal loading over the Vulcan XC72 high-surface-area carbon substrate was in both cases 20 wt%. Hereafter, PtM/C will denote either the one or the other material, unless otherwise specified.

All the electrochemical experiments (characterization and accelerated stress test procedures) were conducted using a computer-controlled numerical potentiostat (Autolab PGSTAT302N).

The dry cell, extensively detailed in Ref. [41], consists of a Kel-F base onto which a Kel-F upside-down U-cup cover is attached. The base supports the polymer electrolyte membrane (Nafion® 115), which separates the working electrode (either the ultramicroelectrode with cavity loaded with the PtM/C powder, or the Lacey carbon membrane TEM gold grid, 300 mesh, Ted Pella, Inc.,®), positioned on the lower side of the membrane, from the Pt-mesh counter-electrode (facing the working electrode, on the upper side of the membrane). A reversible hydrogen electrode (RHE, reference electrode) is maintained in contact with the Nafion® membrane by its capillary tip, which enables ionic percolation with the working electrode. The tip of the RHE is located *ca.* 2 cm away from the working electrode and on the other side of the polymer membrane, to avoid its contamination by the aqueous H<sub>2</sub>SO<sub>4</sub> electrolyte of the RHE. During the whole experiment (aging or characterization procedure), the cell is fed with fully humidified gases (argon or oxygen, all in high purity, Air Liquide®) on both side of the membrane. The classical 3-electrode cell used for experiments in liquid electrolyte is detailed in Ref. [31].

The single PEMFC tests were performed using membrane electrode assemblies based on a Nafion® 115 membrane (geometric electrode area: 4.6 cm<sup>2</sup>). The cathode was loaded with either Pt<sub>3</sub>Co/C or with Pt/C, the Pt loading being kept identical in all cases. It was operated at *T* = 353 K (*i.e.*, 55 K above the temperature at which the AST and the characterizations were performed in liquid electrolyte and in the dry cell) and fed with fully hydrated H<sub>2</sub>/O<sub>2</sub> (1 atm/1 atm) or fully hydrated H<sub>2</sub>/N<sub>2</sub> (1 atm/1 atm) during the acquisition of the polarization curves and AST, respectively. CO stripping voltammograms were also plotted by feeding the cell with fully hydrated H<sub>2</sub>/CO (1000 ppm) followed by N<sub>2</sub> in the working (positive) electrode and H<sub>2</sub> in the counter and reference (negative) electrode. The potential program and duration of the sequences under H<sub>2</sub>/CO and N<sub>2</sub> at the working electrode were kept identical as in the dry cell or liquid electrolyte environment [31,41].

### 2.2. Electrochemical procedures

The accelerated stress test (AST) performed on the Pt/C and Pt<sub>3</sub>Co/C working electrode consists of alternated 60 s-long steps at low (*E*<sub>low</sub> = 0.1 or 0.6 V vs. RHE) and high (*E*<sub>high</sub> = 0.9 V vs. RHE) potential during 15 h at room temperature (*T* = 298 ± 2 K). In general, the AST were performed under argon atmosphere, but a test was also conducted under O<sub>2</sub> atmosphere in a last set of

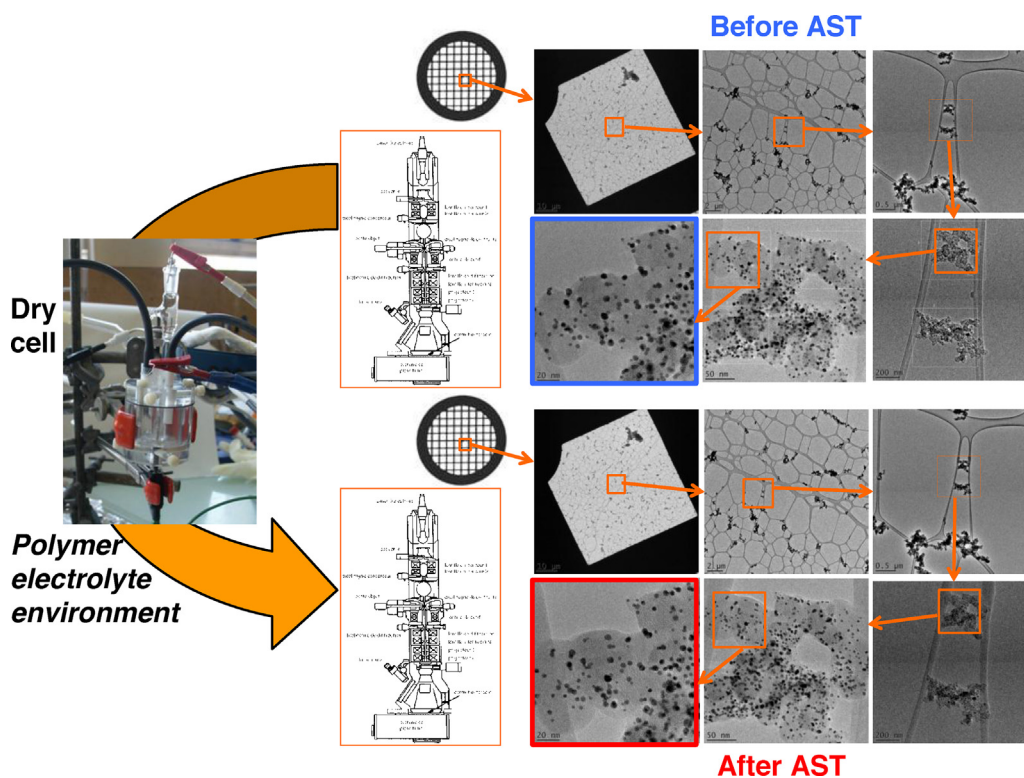


**Fig. 1.** Principle of the identical-location transmission electron microscopy (IL-TEM) in polymer electrolyte environment. The same region of the electrocatalyst deposited on the gold TEM grid is observed in TEM prior/after accelerated stress test (AST) performed in the dry cell.

experiment, to investigate the fate of the PtM/C electrocatalyst under stronger oxidizing environment. The electrochemical characterizations applied prior/after the AST consisted of a CO stripping voltammogram (performed in  $1 \text{ mol L}^{-1} \text{ H}_2\text{SO}_4$  solution, see Ref. [41] for details) to measure the electroactive area of the PtM/C nanoparticles, and a quasi-stationary ( $1 \text{ mV s}^{-1}$ ) oxygen reduction voltamperometry between  $E = 1.05$  and  $0.3 \text{ V}$  vs. RHE to probe their intrinsic ORR activity. Overall, the procedures are similar to those performed in Ref. [31], except Nafion® polymer electrolyte is used instead of  $1 \text{ mol L}^{-1}$  sulfuric acid solution: the working electrode remained at the interface with a 115 Nafion® membrane in the absence of any liquid electrolyte during the whole AST and ORR characterizations. In all cases (dry cell and aqueous  $\text{H}_2\text{SO}_4$  electrolyte solution), the temperature was similar ( $T = 298 \pm 2 \text{ K}$ ) during the AST and ORR characterization, which enables comparing the tests on the basis of the presence/absence of excess liquid water.

For comparison, similar tests were performed with membrane electrode assemblies bearing a PtM/C cathode operated in unit-cell PEMFC and in liquid electrolyte (see Ref. [31]).

We finally point out that, the AST conducted in the present contribution are not designed to be absolutely representative of PEMFC operation, and that the degradations monitored herein cannot be

directly extrapolated to predict what would happen upon a real long-term PEMFC test on the field.

### 2.3. Identical location TEM (IL-TEM) procedures

The TEM micrographs were obtained on a JEOL 2010 TEM apparatus, equipped with a LaB<sub>6</sub> filament operating at 200 kV (point to point resolution  $0.19 \text{ Å}$ ) and an X-ray energy dispersive spectrometer: X-EDS, Oxford – INCA®.

In the IL-TEM experiments, a suspension of  $1 \text{ g}_{\text{PtM/C}} \text{ L}^{-1}$  of PtM/C, composed of 5 wt% Nafion® solution (Aldrich) in 1:0.63 dry weight ratio, MQ-grade water and 20 wt% Pt<sub>3</sub>Co/C, was ultrasonically mixed for 30 min to obtain a well-dispersed ink. An aliquot of  $5 \mu\text{L}$  was then deposited on a gold TEM grid and dried in air. The TEM grid bearing the catalytic ink composed of PtM/C powder and Nafion® was used as the working electrode in the dry cell and kept in contact with the Nafion® 115 polymer electrolyte during the AST and the electrochemical characterizations (Fig. 1).

The overall sequence of electrochemical characterizations/AST was kept identical whatever the nature of the working electrode (UMEC or TEM grid). The TEM images were used to qualitatively observe the changes of particles shape (change of sphericity, extent

**Table 1**  
Mean Pt/C and Pt<sub>3</sub>Co/C electrochemical surface area (ECSA/ $\text{cm}^2$  of Pt, measured from the CO-stripping CV of Fig. 3) and its variation upon the AST ( $\Delta(\text{ECSA})$ ) measured for PtM/C UMEC before and after the various AST performed in the dry cell (Ar or O<sub>2</sub> atmosphere during the AST).

Sample	Pt <sub>3</sub> Co/C		Pt/C	
	AST protocol and atmosphere		AST protocol and atmosphere	
	0.1–0.9 V Ar	0.6–0.9 V Ar	0.1–0.9 V Ar	0.6–0.9 V Ar
ECSA before <sup>a</sup>	$3.57 \cdot 10^{-7}$	$4.55 \cdot 10^{-7}$	$2.62 \cdot 10^{-7}$	$3.71 \cdot 10^{-7}$
ECSA after <sup>a</sup>	$3.45 \cdot 10^{-7}$	$4.38 \cdot 10^{-7}$	$1.70 \cdot 10^{-7}$	$3.31 \cdot 10^{-7}$
$\Delta(\text{ECSA})$	–3.4%	–3.7%	–35%	–11%

<sup>a</sup> The ECSA is given in absolute value (in  $\text{cm}^2$  for the whole PtM/C UMEC), and must only be considered comparatively before/after the AST for a given sample, because controlling precisely the amount of PtM/C powder inserted in the UMEC cavity is not possible due to difficulties to compact the catalyst powder in the cavity in a reproducible manner.

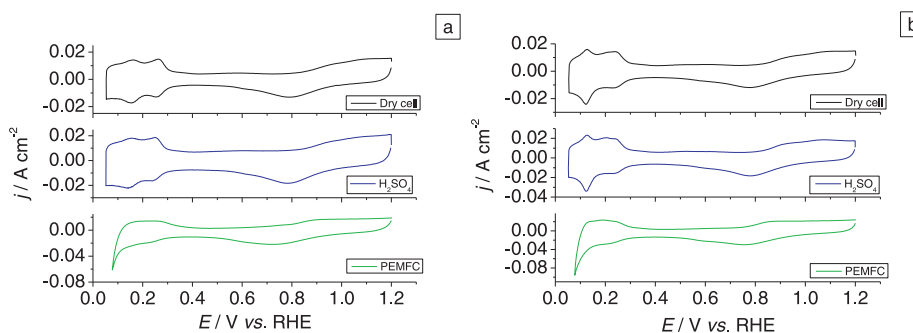


**Fig. 2.** Cyclic voltamperogram measured in “supporting electrolyte” for (a) a  $\text{Pt}_3\text{Co/C}$  UMEC and (b) a  $\text{Pt/C}$  UMEC in contact with (black curve) a Nafion® 115 membrane in the dry cell, (blue curve) 1 M  $\text{H}_2\text{SO}_4$  aqueous electrolyte and (green curve) a Nafion® 115 membrane in unit PEMFC. (For interpretation of the references to color in figure legend, the reader is referred to the web version of this article.)

of agglomeration) and distribution over the carbon substrate, and to quantitatively follow the number and size of the nanoparticles in similar regions of the Vulcan XC72 carbon prior/after the AST.

From the IL-TEM micrographs, particle size distribution histograms were reconstructed, by counting several tenths of isolated (i.e., not agglomerated) nanoparticles precisely the same regions of the samples prior and after the AST. For clarity, it has been decided to quantitatively enumerate the PtM/C nanoparticles only for the IL-TEM micrographs presented throughout the paper. Doing so, we evaluated in a quantitative manner (i) the overall amount of nanoparticles in the considered region (to quantify nanoparticles appearance – e.g., by Pt redeposition following Pt (or PtM) dissolution/disappearance – e.g., by dissolution and/or detachment from the carbon substrate), (ii) the shape of the carbon substrate, (iii) the shape and size (diameter) of the nanoparticles and (iv) for  $\text{Pt}_3\text{Co/C}$  nanoparticles, their local composition (Pt and Co at%). From these data, number-averaged ( $d_N$ ), surface-averaged ( $d_S$ ), volume-averaged ( $d_V$ ) particles diameters were calculated (see Refs. [6,18] for details).

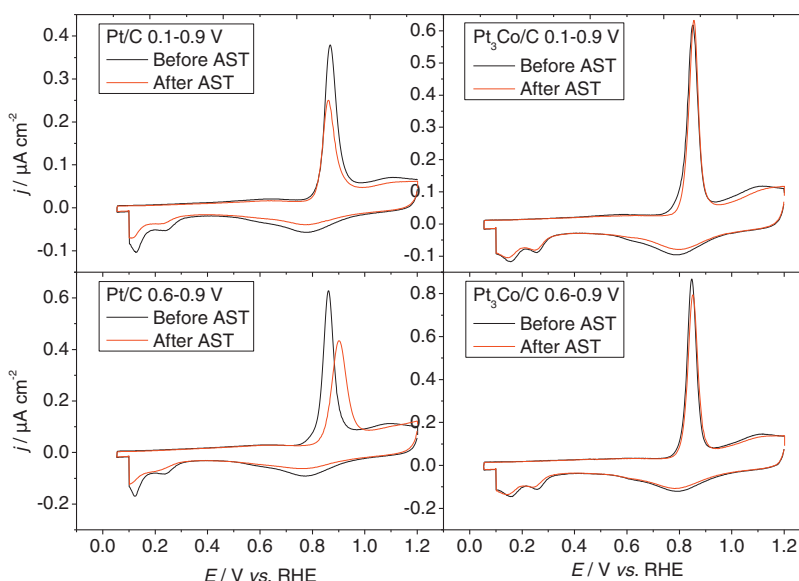
### 3. Results and discussion

Fig. 2 shows typical cyclic voltamperogram measured in “supporting electrolyte” for (a) a  $\text{Pt}_3\text{Co/C}$  UMEC and (b) a  $\text{Pt/C}$  UMEC, in contact with a Nafion® 115 membrane in the dry cell, 1 M  $\text{H}_2\text{SO}_4$  aqueous electrolyte in a classical three-electrode electrochemical

cell and a Nafion® 115 membrane in a unit PEMFC. The plots demonstrate the rather similar behavior of the two PtM/C electrocatalysts in the liquid aqueous solution and solid polymer electrolyte environments, at least for similar working electrodes (PtM/C UMEC); in PEMFC environment, the hydrogen region ( $0.05 < E < 0.35$  V vs. RHE) is less-defined than for the PtM/C UMEC, but this is classically explained by additional capacitive and Ohmic effects as well as to the inherent two-electrode setup in the MEA configuration [2,3,7].

The first cycle of the CO-stripping voltamperograms of Fig. 3 further enables to characterize the two commercial electrocatalysts nanoparticles, both before and after the two accelerated stress-test (AST) performed under Ar atmosphere. As the current densities in Fig. 3 are presented with respect to the geometric surface area of the UMEC, the variation of the area under the CO-stripping peak directly reveals the extent of electrochemical surface area (ECSA) loss upon the AST (the values of ECSA before/after the AST, as well as of the ECSA variation upon the AST,  $\Delta(\text{ECSA})$ , are summarized in Table 1). Overall, whatever the AST and the electrocatalyst considered, the electrochemical area of electrocatalyst contained in the UMEC decreases after the AST. This decrease is however much more pronounced for  $\text{Pt/C}$  than for  $\text{Pt}_3\text{Co/C}$ . In the latter case, the CO-stripping CV only slightly changes upon the AST, in agreement with the negligible ECSA variations.

In addition, for  $\text{Pt/C}$  the decrease after the 0.1–0.9 V vs. RHE aging procedure exceeds that after the 0.6–0.9 V vs. RHE aging procedure, these changes being accompanied with appreciable modifications



**Fig. 3.** 1st cycle of the CO-stripping CV measured for UMEC with  $\text{Pt/C}$  and  $\text{Pt}_3\text{Co/C}$  electrocatalysts before/after AST performed in the dry cell under Ar atmosphere.

**Table 2**  
Mean number-averaged ( $d_N$ ), surface-averaged ( $d_S$ ) and volume-averaged ( $d_V$ ) Pt/C and Pt<sub>3</sub>Co/C particle diameter ( $d_N$ ,  $d_S$  and  $d_V$  / nm), alloy composition (at% Co, derived from X-EDS measurements under the TEM beam) measured by IL-TEM before and after the various AST performed in the dry cell (Ar or O<sub>2</sub> atmosphere during the AST). The last line of the table presents the variation of the number of metallic nanoparticles detected of the selected carbon grains prior / after the AST ( $\Delta n$  / %).

	Sample/AST protocol and atmosphere	Pt <sub>3</sub> Co/C		Pt/C	
		0.1–0.9 V Ar	0.6–0.9 V Ar	0.1–0.9 V O <sub>2</sub>	0.6–0.9 V O <sub>2</sub>
$d_N$	Before	3.45 ± 0.12	3.46 ± 0.12	–	–
	After	3.56 ± 0.13	3.45 ± 0.14	–	–
$d_S$	Before	3.87 ± 0.12	3.80 ± 0.12	–	–
	After	3.95 ± 0.13	3.82 ± 0.14	–	–
$d_V$	Before	4.06 ± 0.12	3.94 ± 0.12	–	–
	After	4.12 ± 0.13	3.97 ± 0.14	–	–
at% Co	Before	18.6 ± 2.2	18.5 ± 4.1	16.3 ± 2.9	–
	After	18.4 ± 3.2	17.8 ± 3.9	16.6 ± 2.5	–
$\Delta n$ / %		–4.2	–21	–34	–11

of the CO-stripping CV, in terms of surface area and of peak potential. Here again, the nature of the AST matters: for Pt/C only a slight negative shift is witnessed after the 0.1–0.9 V vs. RHE AST, suggesting a slight increase of the average Pt nanoparticle size [47]; thus, the pronounced ECSA loss observed in that case must be related to some Pt nanoparticles losses (e.g., by detachment from the carbon surface, following carbon corrosion), but more to Pt nanoparticles irreversible dissolution and (partial?) redeposition. On the contrary, after the 0.6–0.9 V vs. RHE AST, the ECSA loss is associated to a sharp positive shift of the CO-stripping peak potential, suggesting that in average, the remaining Pt nanoparticles after the AST are smaller than before: irreversible dissolution of Pt must have been non-negligible here, in agreement to what was observed in liquid electrolyte in Ref. [31]. The evolution of the Pt-oxide reduction peaks in the negative scans of the CO-stripping CV in Fig. 3 are in agreement with these observations.

Figs. 4–7, show representative micrographs of the Pt<sub>3</sub>Co/C (Figs. 4 and 5) and Pt/C electrocatalysts (Figs. 6 and 7) obtained in identical-location TEM before/after the 0.1–0.9 V vs. RHE and the 0.6–0.9 V vs. RHE aging procedure, respectively. The variations of the corresponding nanoparticles size distribution histograms (PSD) is also included in the figures (in average 50–100 nanoparticles were counted for the PSD, from the two representative micrographs taken at a magnification of  $\times 200,000$  presented in Figs. 4–7 for the various experiments). Compared to the similar figures obtained in liquid electrolyte environment in Ref. [31], one observes that all the mechanisms of degradation of the PtM/C nanoparticles observed (see the representative markers on the figures) are still at stake in polymer electrolyte environment. However, a closer look at the figures reveals that (i) the extent of degradation in a given AST for a given electrocatalyst is smaller in polymer electrolyte environment than in liquid electrolyte, (ii) the prevalent degradation mechanisms are not the same in the two environments and that (iii) the degradations observed are more heterogeneous from one region of the electrocatalyst in polymer electrolyte environment, following the smaller utilization and effectiveness factors of the electrocatalysts in polymer electrolyte environment [26,48]. These features were essentially already noted in [41] for the particular case of Pt<sub>3</sub>Co/C before/after the 0.1–0.9 V vs. RHE aging procedure. Table 2 summarizes the mean particle diameters, composition and number of nanoparticles in the regions investigated for the PtM/C electrocatalysts before/after these tests, all determined from the IL-TEM micrographs. To be more precise, the degradations phenomena highlighted on Figs. 4–7, in the various case studies are as follows.

For the 0.1–0.9 V vs. RHE AST under Ar atmosphere, Fig. 4 reveals that the three main markers of degradation of the Pt<sub>3</sub>Co/C nanoparticles are particles detachment from the carbon substrate (yellow dashed line), the coalescence of nanoparticles (white dashed double-dot line) and the electrochemical deposition of Pt nanoparticles (red line). Carbon corrosion (green lines) is also directly witnessed by the change of outline of some carbon grains, but this is less spectacular than in liquid electrolyte conditions for the same AST and sample [31]. The most striking difference with the AST in liquid electrolyte though, is the major evidence of Pt electrochemical deposition in polymer electrolyte, which in our previous contribution [41] was associated to the easier redeposition of Pt<sup>2+</sup> cations trapped in the Nafion® polymer electrolyte than when these cations can escape the interfacial region by bulk diffusion in the excess liquid electrolyte. Associated to this non-negligible Pt redeposition, one clearly sees that some particles change of size and shape (blue dashed line), probably because Pt redeposition “connects” pre-existing nuclei (an indirect sign of (electrochemical) Ostwald ripening).

When the lower vertex potential of the AST is set at  $E_{low} = 0.6$  V vs. RHE (Fig. 5), whereas evidences of nanoparticles migration over the carbon substrate (either coalescence or separation: orange

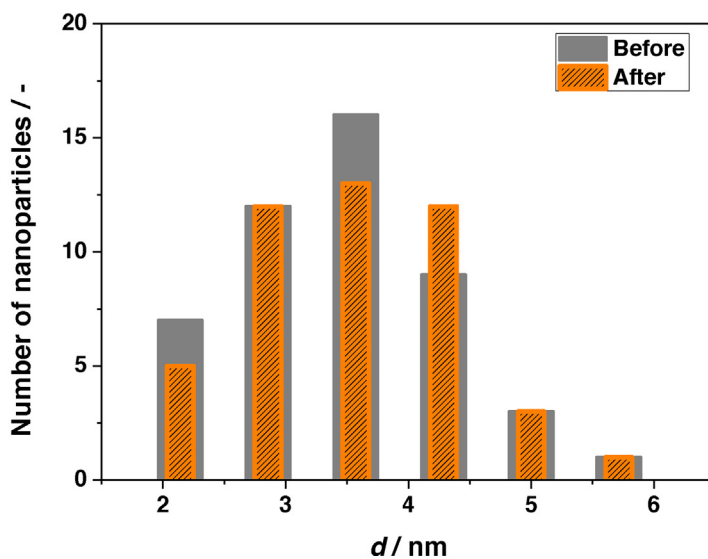
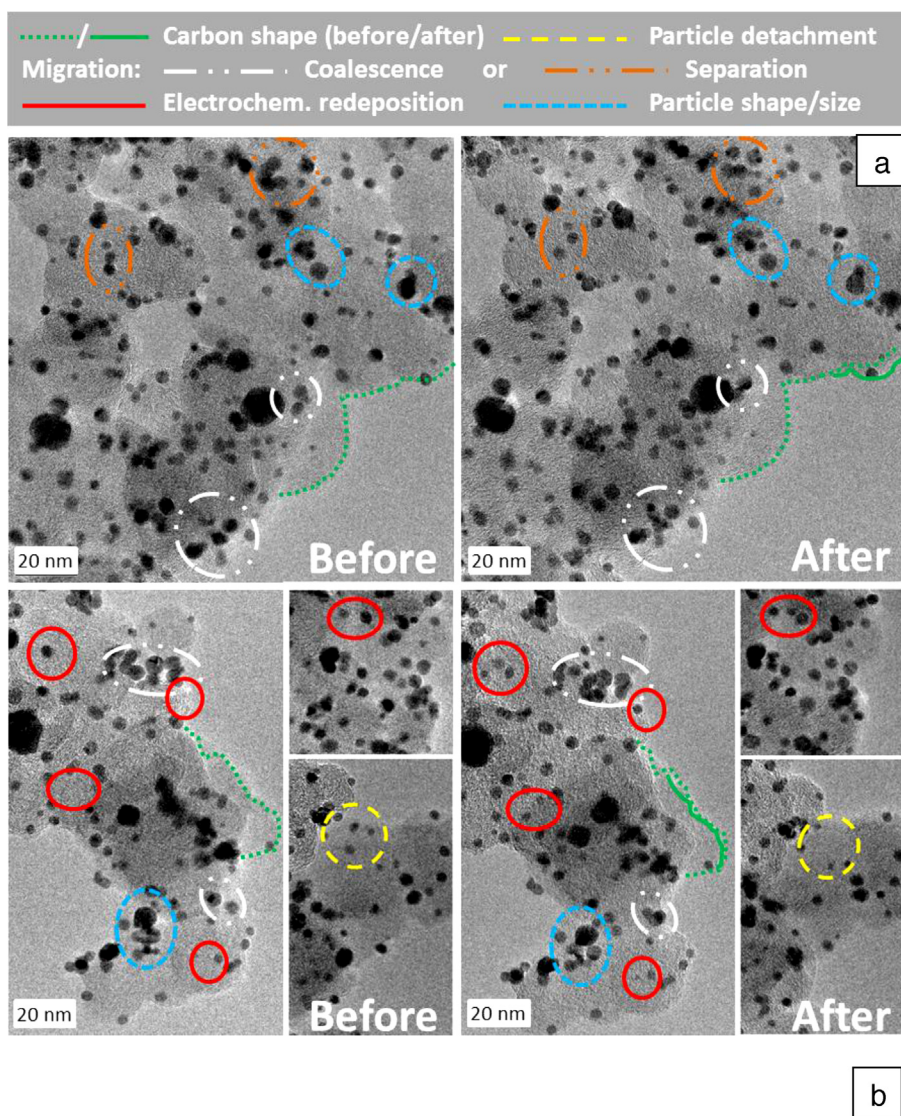


**Fig. 4.** (a) IL-TEM images of Pt<sub>3</sub>Co/C nanoparticles before and after ageing in dry cell (Nafion® 115 electrolyte) in the 0.1–0.9 V vs. RHE protocol under Ar atmosphere and (b) corresponding particle size distribution histograms. The (non-comprehensive) markers on the figure highlight representative examples of aging phenomena that occurred during the AST. Micrographs reproduced from Ref. [41] with permission from Elsevier. (For interpretation of the references to color in text, the reader is referred to the web version of this article.)

dashed double-dot line), particles detachment and carbon corrosion are observed, literally no sign of electrochemical redeposition is witnessed (and neither any of particles with changed size/shape), as expected when no incursion of the electrode potential is made in the Pt-reduction region: in other words, the formed  $\text{Pt}^{2+}$  cations do not redeposit when the electrode potential always exceeds  $E_{\text{low}} = 0.6 \text{ V}$  vs. RHE during the AST.

If one now focusses on the fate of non-containing Co electrocatalysts in the same AST than above, one firstly has to recognize that the exact same markers of degradation are observed at given condition for Pt/C and  $\text{Pt}_3\text{Co}/\text{C}$  (compare Fig. 6 to Fig. 4 for the 0.1–0.9 V vs. RHE test, and Fig. 7 to Fig. 5 and for the 0.6–0.9 V vs. RHE test). When the smaller low-vertex potential of  $E_{\text{low}} = 0.1 \text{ V}$  vs. RHE is employed, Pt redeposition is non-negligible (and for Pt/C again, much more pronounced than in liquid aqueous electrolyte [31]), while absent for the larger low-vertex potential ( $E_{\text{low}} = 0.6 \text{ V}$  vs. RHE). Besides, it seems that the markers associated to the corrosion of carbon (either direct: green lines, or indirect: detachment: yellow dashed line, migration: white and orange dashed double-dot lines) are prevalent when the electrocatalysts nanoparticles only contain Pt. This effect was already observed after AST performed in liquid aqueous electrolyte [31] and was associated to the role of “sacrificial anode” of the Co atoms of  $\text{Pt}_3\text{Co}/\text{C}$  nanoparticles. In other words, when Co is present in the sample, it is oxidized and leached preferentially (it plays the role of a sacrificial anode), therefore “consuming” the anodic charge at the benefit of platinum and carbon corrosion, the two latter elements being “protected” (as long as Co remains). One would however note that the Co content of the samples does not seem to evolve much before/after the AST (it is essentially stable or only slightly decreasing upon AST: Table 2), but the authors point out that X-EDS cannot give specific insight into the proportion of Co that remains alloyed in the  $\text{PtCo}/\text{C}$  nanoparticles. As previously observed in [28], the authors believe that Co is indeed corroded (into  $\text{Co}^{3+}$ ), but the latter moieties remain trapped in the solid ionomer, thereby impeding their diffusion away from the interface (such bias is much less prevalent when excess water is present in liquid aqueous electrolyte environment and can dilute the  $\text{Co}^{3+}$  species).

In the case of Pt/C for both AST and for  $\text{Pt}_3\text{Co}/\text{C}$  after the 0.1–0.9 V vs. RHE, the nearly-identical values of  $\Delta(\text{ECSA})$  and  $\Delta n$  in Tables 1 and 2, respectively, demonstrate that the losses of ECSA may mainly be attributed to loss of PtM/C nanoparticles (either from irreversible detachment, dissolution or migration followed by coalescence). On the contrary, the nanoparticles growth is not dramatic in polymer electrolyte environment, when compared to what proceeds in liquid electrolyte [31]: the nanoparticles diameter increase remains below 3% in all cases, except for Pt/C upon the 0.1–0.9 V vs. RHE AST, where the growth is much more pronounced: +20%.

Overall, the degradations monitored in IL-TEM in polymer electrolyte environment resemble those detected upon similar AST performed in unit PEMFC (see Figs. S1 and S2 in Supplementary information). Moreover, as noticed in [41], in both cases, the degradations observed are heterogeneous from one region (typically one carbon grain) to another, which can be linked to imperfect utilization and effectiveness factors in solid electrolyte, as widely demonstrated in the recent literature [22,23,25,28,48–50].

To summarize the general observations derived from the IL-TEM micrographs, one notes that the particle size growth, particles agglomeration, particles loss, carbon corrosion, losses of Co are all minored after AST in polymer electrolyte versus liquid aqueous electrolyte environment. The only marker that is more pronounced in polymer electrolyte vs. aqueous liquid environment is the particles electrochemical (re)deposition, but this process is only observed when the smaller vertex potential of the AST is set at  $E_{\text{low}} = 0.1 \text{ V}$  vs. RHE. One other conclusion derived of these tests,

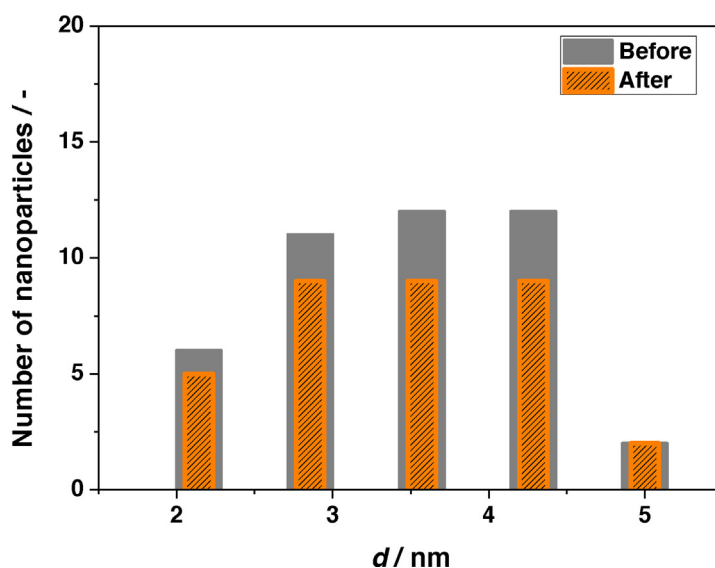
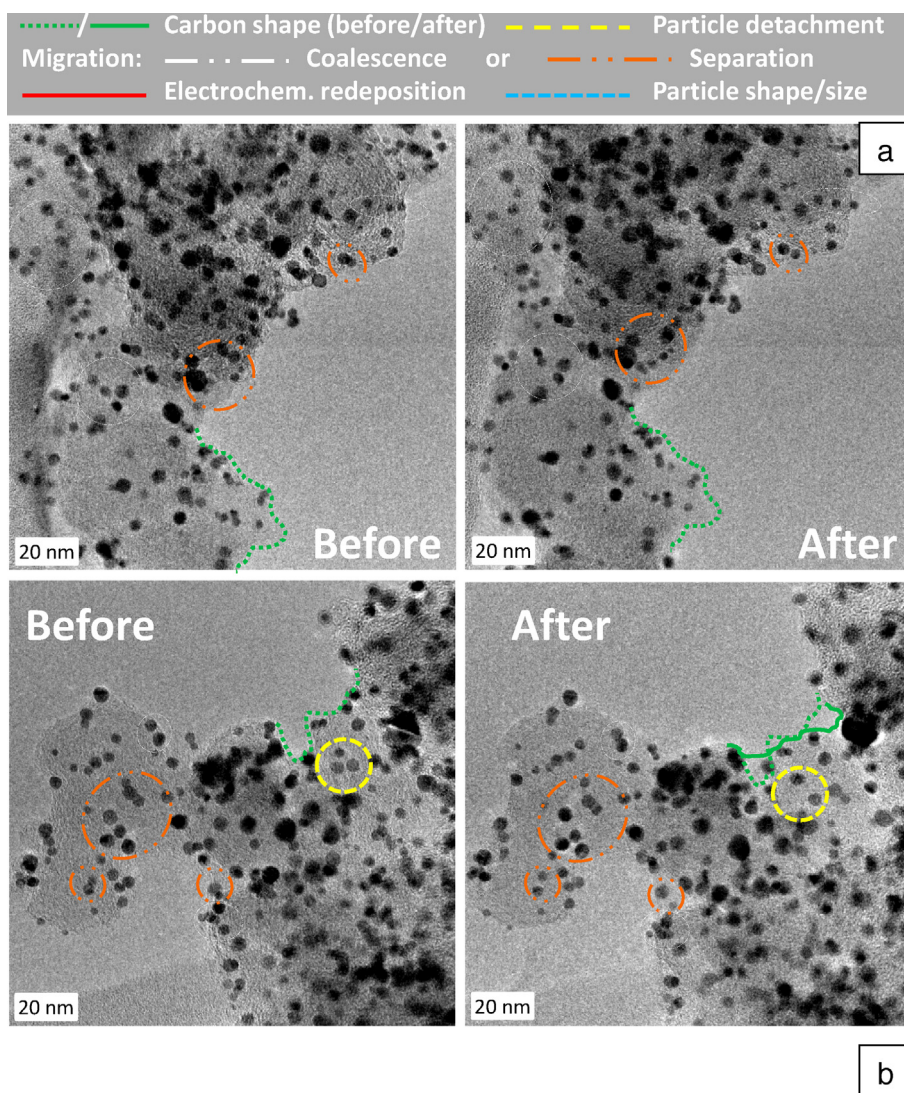
is that the presence of the cobalt atoms in  $\text{Pt}_3\text{Co}/\text{C}$  nanoparticles minors the corrosion of carbon and platinum, which can be attributed to the role of “sacrificial anode” played by Co in such samples, and was already observed in liquid electrolyte [31].

Beyond monitoring the degradation mechanisms of the PtM/C samples in the various AST, of prime importance was to link the observed degradations to the change of oxygen reduction reaction performance of the electrocatalysts. For that purpose, ultramicro-electrodes with cavity (UMEC) of the electrocatalysts were tested with the same electrochemical protocol (same characterizations, same AST) in the dry cell. We emphasize at this point that the UMEC data obtained in the dry cell must be viewed as a means to compare a given electrode prior/after the AST, more than a manner to measure with precision the ORR kinetics parameters of the electrocatalyst immobilized in the UMEC, as put into evidence by the discrepancies between the initial SA values (Table 3) measured for different UMECs.

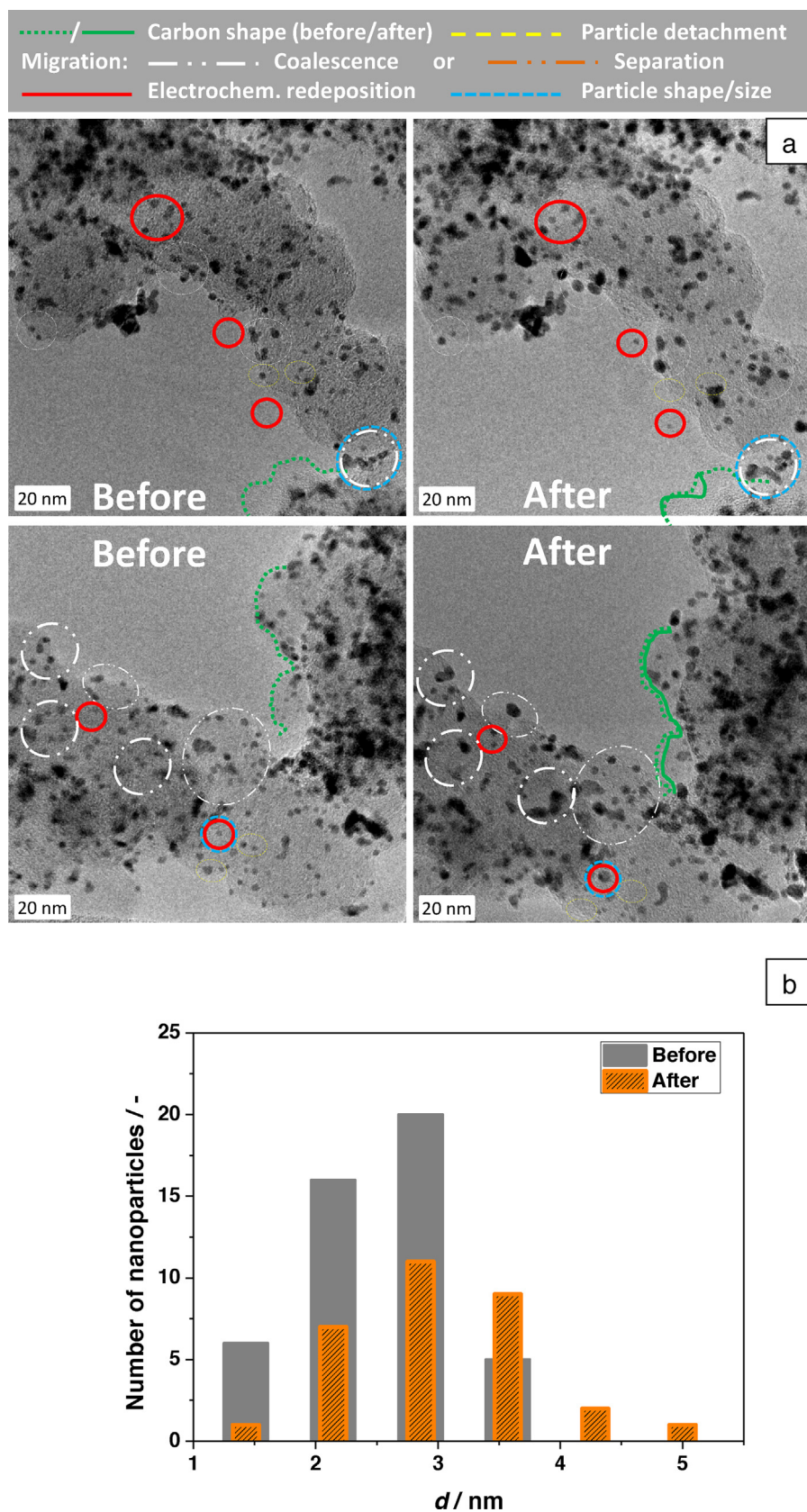
Fig. 8 shows the corresponding ORR voltamperograms, plotted with respect to the geometric area of the UME cavity: in all cases the apparent ORR activity of the PtM/C samples decrease after the AST, except for Pt/C after the 0.1–0.9 V vs. RHE test. In the case of Pt/C after the 0.1–0.9 V vs. RHE test, the ORR performance improvement agrees with that observed in liquid electrolyte; this may be accounted for by the small but non-negligible increase of the mean particle size indirectly observed on the CO-stripping CV of Fig. 3(a) (the smallest particles are eliminated at the benefit of the larger ones, by 3D Ostwald ripening) and directly witnessed in Table 2, which is beneficial to the ORR activity (the well-known Pt particle-size effect [13]). When the lower vertex potential of the AST prevents Pt redeposition ( $E_{\text{low}} = 0.6 \text{ V}$  vs. RHE), the ORR activity is strongly depreciated, both for Pt/C and  $\text{Pt}_3\text{Co}/\text{C}$  electrocatalysts. In particular, the strong depreciation of the ORR activity of the  $\text{Pt}_3\text{Co}/\text{C}$  sample after the 0.1–0.9 V vs. RHE test denotes for antagonist effects: whereas Pt redeposition is promoted (and observed, see Fig. 4) at the lowest vertex potential of the AST ( $E_{\text{low}} = 0.1 \text{ V}$  vs. RHE), Co dissolution and associated formation of  $\text{Co}^{3+}$  cations proceed regardless of the potential witnessed by the working electrode. Therefore, the beneficial alloying effect of Co to Pt is irreversibly lost, adversely affecting the intrinsic activity of the remaining alloy (depleted in Co) [30]. In addition, the  $\text{Co}^{3+}$  cations generated are not capable to redeposit in the environment of a polymer electrolyte fuel cell [18,19]. Therefore, these  $\text{Co}^{3+}$  species remain trapped in the ionomer (see above and in Refs. [28,41]), adversely affecting the mass-transport of protons and oxygen molecules to the metal | solid polymer interface [27], which ultimately severely decreases the apparent ORR performances of the  $\text{Pt}_3\text{Co}/\text{C}$  electrocatalyst [41]. The other main degradation phenomena observed in the IL-TEM in polymer electrolyte environment (particles migration: coalescence and separation and carbon corrosion) negligibly affect the ORR voltamperograms of Fig. 8. Finally, in terms of ORR specific activity (SA, which is the current density measured at 0.85 or 0.9 V vs. RHE divided by the present ECSA of the electrocatalyst, Table 3), the general trends monitored on Fig. 8 are maintained. Despite the overall minor materials degradation observed in polymer electrolyte environment (see Figs. 4–7), the depreciation of the ORR SA values is significant (except for Pt/C in the 0.1–0.9 V vs. RHE test). In that way, the milder aging of the PtM/C electrocatalysts in polymer electrolyte environment compared to that observed in liquid aqueous electrolyte has much larger consequences on the ORR SA; this is mainly due to the detrimental pollution of the ionomer by metal cations ( $\text{Co}^{3+}$  whatever the vertex potentials in the AST and  $\text{Pt}^{2+}$  for the 0.6–0.9 V vs. RHE test).

The picture in PEMFC unit cell (Fig. 9) slightly differs to what was observed in the UMEC configuration.

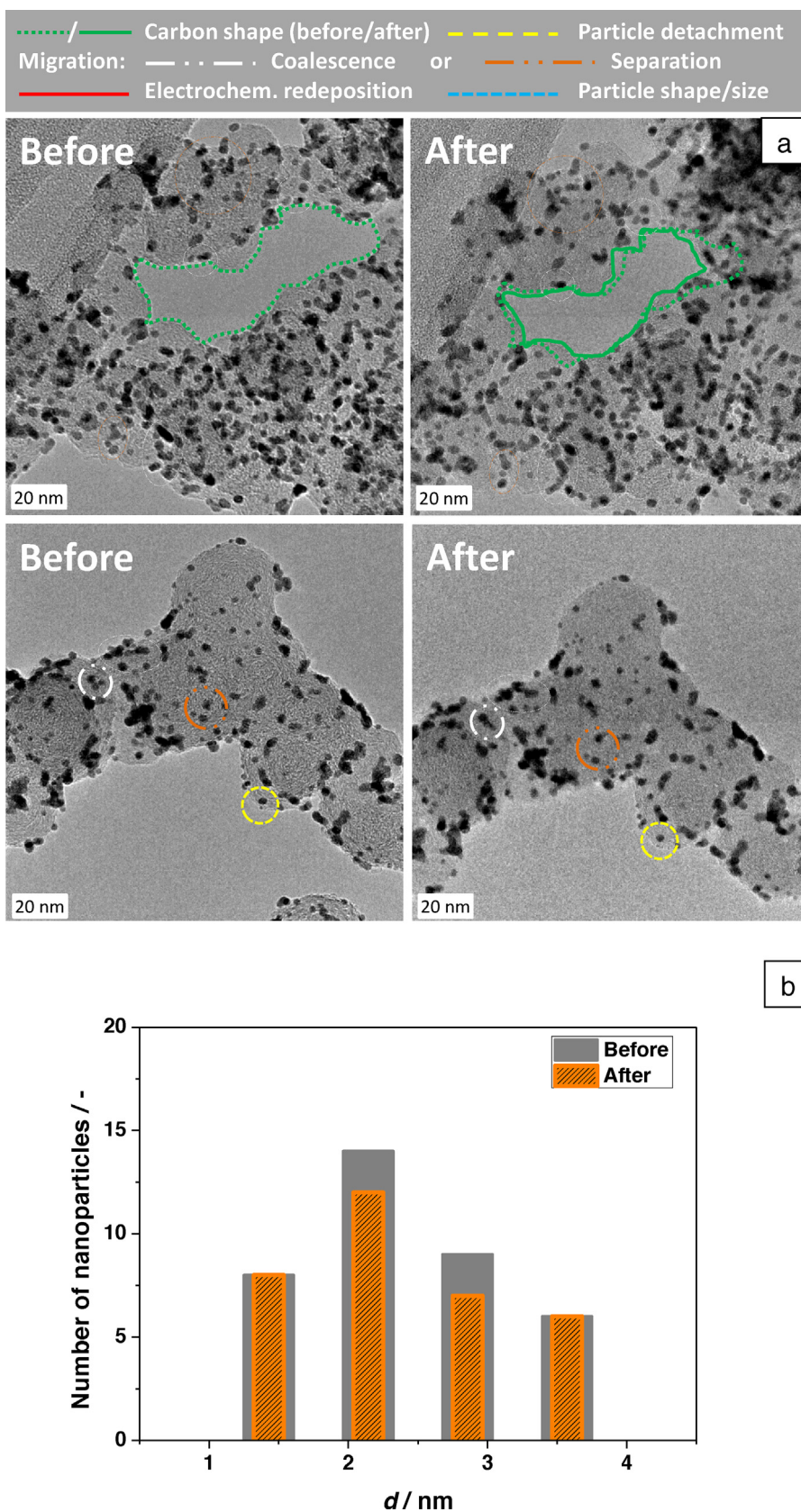
When staring at the “kinetics region” ( $j < 0.2 \text{ A cm}^{-2}$ ) of the ohmic-drop-corrected polarization plots, one sees the different



**Fig. 5.** (a) IL-TEM images of Pt<sub>3</sub>Co/C nanoparticles before and after ageing in dry cell (Nafion® 115 electrolyte) in the 0.6–0.9 V vs. RHE protocol under Ar atmosphere and (b) corresponding particle size distribution histograms. The (non-comprehensive) markers on the figure highlight representative examples of aging phenomena that occurred during the AST. (For interpretation of the references to color in text, the reader is referred to the web version of this article.)



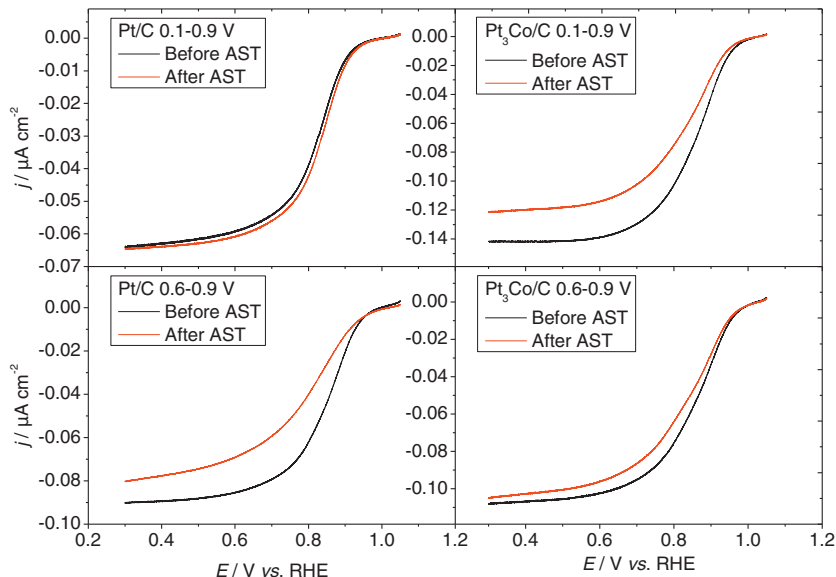
**Fig. 6.** (a) IL-TEM images of Pt/C nanoparticles before and after ageing in dry cell (Nafion® 115 electrolyte) in the 0.1–0.9 V vs. RHE protocol under Ar atmosphere and (b) corresponding particle size distribution histograms. The (non-comprehensive) markers on the figure highlight representative examples of aging phenomena that occurred during the AST. (For interpretation of the references to color in text, the reader is referred to the web version of this article.)



**Fig. 7.** (a) IL-TEM images of Pt/C nanoparticles before and after ageing in dry cell (Nafion® 115 electrolyte) in the 0.6–0.9 V vs. RHE protocol under Ar atmosphere and (b) corresponding particle size distribution histograms. The (non-comprehensive) markers on the figure highlight representative examples of aging phenomena that occurred during the AST. (For interpretation of the references to color in text, the reader is referred to the web version of this article.)

**Table 3**Specific activity (SA in  $\mu\text{A}/\text{cm}^2_{\text{Pt}}$ ) of the Pt/C and  $\text{Pt}_3\text{Co}/\text{C}$  electrocatalysts before and after the various AST performed in the dry cell (Ar atmosphere during the AST).

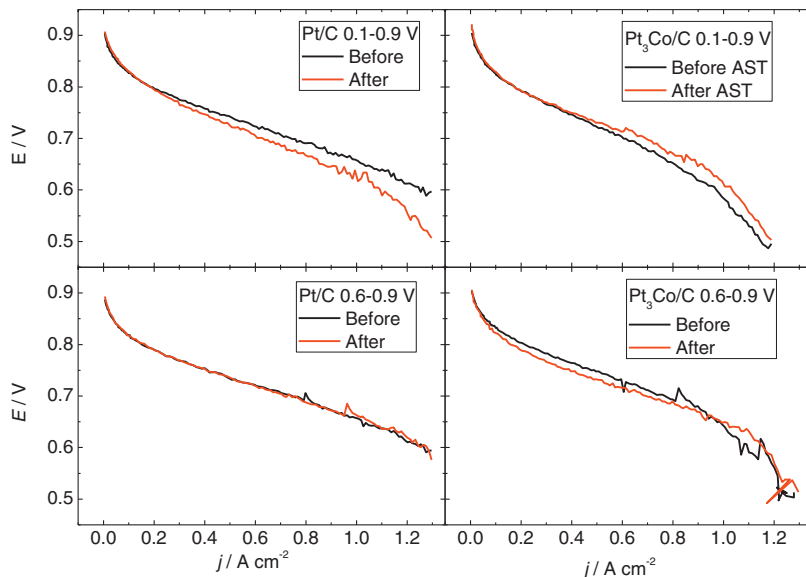
AST protocol	SA @ 0.90 V				SA @ 0.85 V			
	0.1–0.9 V Before	After	0.6–0.9 V Before	After	0.1–0.9 V Before	After	0.6–0.9 V Before	After
Pt/C	2.6	4.9	5.6	3.8	8.4	15	12	8.0
$\text{Pt}_3\text{Co}/\text{C}$	17	11	11	9.0	56	32	30	23

**Fig. 8.** Oxygen reduction reaction (ORR) voltamperogram measured for UMEC with Pt/C and  $\text{Pt}_3\text{Co}/\text{C}$  electrocatalyst in the dry cell before/after AST performed in the dry cell under Ar atmosphere.

fates of the electrocatalysts in the two AST. The catalytic activity of Pt/C unambiguously improves in the 0.1–0.9 V test, and remains essentially unchanged for the 0.6–0.9 V vs. RHE test, as well as for  $\text{Pt}_3\text{Co}/\text{C}$  in the 0.1–0.9 V test. In the latter case, the difference with the observation in the UMEC configuration may be accounted for by the fact that regions of the catalytic layer may activate over time (in line with the incomplete utilization and effectiveness factors of PEMFC electrodes [26,48]); in addition, the convection of

the hydrated gases at high temperature (the PEMFC operates at 353 K versus 298 K in the UMEC) could enable the better removal of poisoning  $\text{Co}^{V+}$  species from the ionomer in PEMFC than in the (static) UMEC configuration. Finally, the kinetics region for  $\text{Pt}_3\text{Co}/\text{C}$  in the 0.6–0.9 V test reveals a non-negligible depreciation of the ORR activity upon aging, in agreement with the UMEC data.

When looking at the high current density region of the polarization plots, the differences of performances before/after the AST are

**Fig. 9.** Ohmic-drop-corrected polarization curves measured for unit PEMFC MEA with Pt/C and  $\text{Pt}_3\text{Co}/\text{C}$  electrocatalysts before/after AST performed in unit PEMFC under Ar atmosphere.

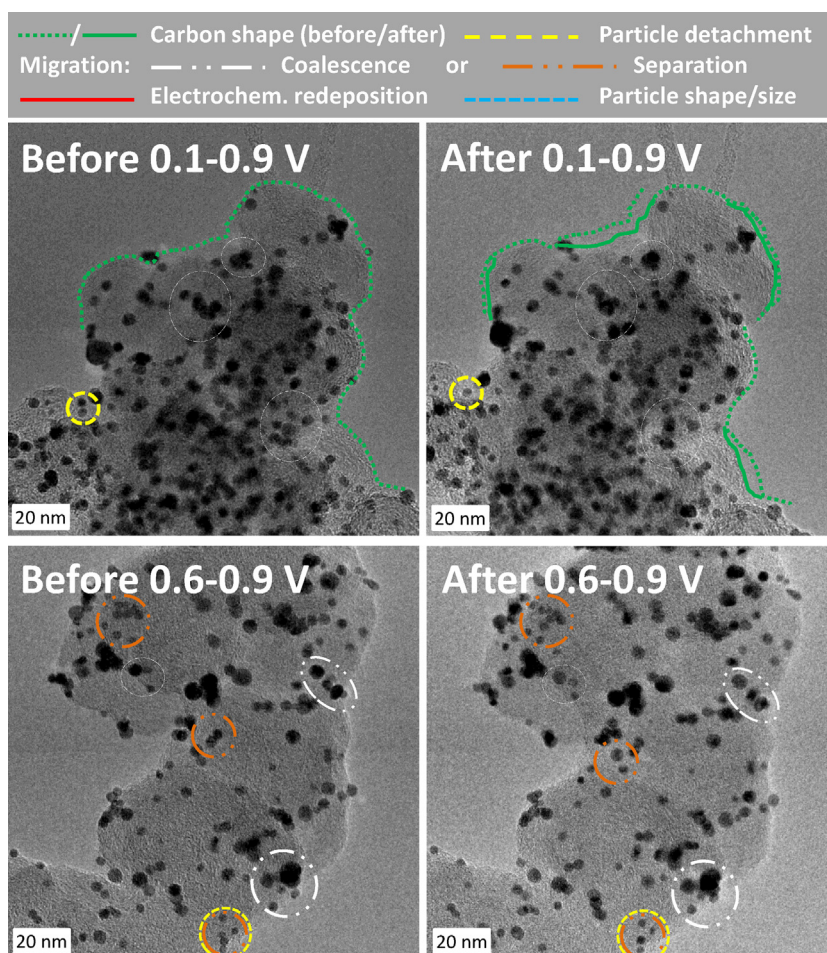


**Fig. 10.** (a) IL-TEM images of Pt<sub>3</sub>Co/C nanoparticles before and after ageing in dry cell (Nafion® 115 electrolyte) under O<sub>2</sub> atmosphere. The (non-comprehensive) markers on the figure highlight representative examples of aging phenomena that occurred during the AST. (For interpretation of the references to color in text, the reader is referred to the web version of this article.)

more marked for the 0.1–0.9 V test than for the 0.6–0.9 V test. In particular, the non-negligible depreciation of performances above  $j = 1 \text{ A cm}^{-2}$  for Pt/C after the 0.1–0.9 V test (whereas in the same test, Pt<sub>3</sub>Co/C MEA maintain – or even slightly improve – their performance) can be associated to detrimental carbon corrosion and associated mass-transport losses (the carbon substrate can become more hydrophilic when it corrodes and therefore more prone to flooding at high current densities, and its severe corrosion destroys the porous structure of the active layers, impeding the reactant/product transport/draining within the active layers), as recently demonstrated after long-term PEMFC operation [22–25]. The corrosion of the carbon substrate is more pronounced when incursions to low-potential values (below the potential of Pt and carbon reduction, which is the case for 0.1 V vs. RHE but not for 0.6 V vs. RHE) are made [51,52] and when “sacrificial metal” is not present, as previously observed in model liquid and solid electrolyte environments [31,41].

Finally, the influence of the atmosphere (and in particular of an oxidizing atmosphere) was checked in IL-TEM for the Pt<sub>3</sub>Co/C catalyst. Fig. 10 demonstrates that having O<sub>2</sub> molecules in contact with this electrocatalyst dramatically affects its fate during the AST.

When the lower vertex potential is set at  $E_{\text{low}} = 0.1 \text{ V}$  vs. RHE, it is clearly observed that Pt electrodeposition, which was the main observed degradation marker for the AST under Ar atmosphere (see red markers in Fig. 4), is literally not taking place under O<sub>2</sub> atmosphere. This shows that either Pt<sub>3</sub>Co dissolution is not dramatic in these conditions or that Pt redeposition is hindered in the presence

of O<sub>2</sub> or of its adsorbates. On the contrary, the signs of crystallite migration and carbon corrosion seem emphasized compared to the case under Ar atmosphere. In other words, the presence of an oxidant atmosphere is detrimental to the carbon substrate (as also observed in liquid electrolyte conditions for Pt/C samples [53]) but not much to the Pt<sub>3</sub>Co nanoparticles.

On the contrary, when the lower vertex potential is set at  $E_{\text{low}} = 0.6 \text{ V}$  vs. RHE, the behavior of the Pt<sub>3</sub>Co/C nanoparticles under O<sub>2</sub> atmosphere is comparable to that observed under Ar atmosphere (see Fig. 5).

#### 4. Conclusion

Through an identical-location transmission electron microscopy (ILTEM) study the morphology and composition of Pt/C and Pt<sub>3</sub>Co/C electrocatalysts was studied before and after electrochemical ageing tests performed in polymer electrolyte environment, using a “dry cell”. Both electrocatalysts suffer modification of their particle size, geometry and composition, these changes depending on the nature of the AST employed. In any case however, the materials degradations observed are much less pronounced than in liquid electrolyte (sulfuric acid solution). This apparent mitigation of the electrocatalysts degradation in polymer environment was attributed to the lack of excess (liquid) water, species that are necessary to corrode carbon and Pt (Pt<sub>3</sub>Co). The nature of the AST also greatly affects the nature and extent of degradations observed: whereas Pt redeposition occurs at  $E_{\text{low}} = 0.1 \text{ V}$  vs. RHE, it is not likely

at  $E_{\text{low}} = 0.6\text{ V}$  vs. RHE, and so extensive particles growth is only observed in the former case for Pt/C. In addition, carbon corrosion is emphasized after incursions at the lower vertex potential, but also when the AST is performed under  $\text{O}_2$  atmosphere instead of Ar. Finally, alloying Pt with Co in  $\text{Pt}_3\text{Co}$  alloys is beneficial to the apparent corrosion of the  $\text{Pt}_3\text{Co}/\text{C}$  nanoparticles, which is explained by the role of sacrificial anode of Co: Co dissolves/corrodes preferentially, therefore decreasing both Pt dissolution from the  $\text{Pt}_3\text{Co}$  nanoparticles and carbon corrosion (in other words, the oxidation current is mainly carried by Co dissolution).

The changes of morphology and composition of the electrocatalysts were further taken into account to explain the changes in ORR intrinsic activity of the electrocatalysts upon electrochemical aging. The ORR activity (measured in the dry cell using an ultramicroelectrode with cavity) only improved for Pt/C nanoparticles aged in the 0.1–0.9 V vs. RHE procedure. It is believed that the increased nanoparticle sizes in these conditions counterbalanced the ECSA loss observed. In all the other cases, the ORR activity decreased upon the AST. For  $\text{Pt}_3\text{Co}/\text{C}$  the positive particle-size effect (triggered by Pt redeposition in the 0.1–0.9 V vs. RHE ageing procedure) is counterbalanced by a detrimental (and large) effect of Co dissolution, which adversely affects the nanoparticles composition for the ORR and pollutes the polymer electrolyte membrane (the  $\text{Co}^{2+}$  cations hinder  $\text{O}_2$  and  $\text{H}^+$  transport in the electrolyte membrane). Finally, the ORR activity always decreases upon the 0.6–0.9 V vs. RHE aging procedure, because the redeposition of Pt is not likely in such conditions; therefore, the positive effect of particle size increase monitored in the 0.1–0.9 V vs. RHE ageing procedure cannot counterbalance the negative effect of Co dissolution (and adverse pollution of the ionomer electrolyte) and ECSA loss.

## Author contributions

The manuscript was written through contributions of all authors. All authors have given approval to the final version of the manuscript.

## Acknowledgment

The authors thank CAPES-COFECUB (Project Ph 598/08) and Oseo H2E for funding. MC thanks the French University Institute (IUF) for its financial support, the UMEC French CNRS network for providing the UMEC, as well as Benoit Vion-Dury, Vincent Vivier and Axel Desnoyers de Marbaix for their participation in the design and realization of the dry cell. This work was performed within the framework of the Centre of Excellence of Multifunctional Architected Materials “CEMAM” no AN-10-LABX-44-01 funded by the “Investments for the Future” Program.

## Appendix A. Supplementary data

Supplementary data associated with this article can be found, in the online version, at <http://dx.doi.org/10.1016/j.apcatb.2015.04.035>.

## References

- [1] A.F. Ghoniem, Prog. Energ. Comb. Sci. 37 (2011) 15–51.
- [2] H.A. Gasteiger, W. Vielstich, H. Yokokawa, Handbook of Fuel Cells, John Wiley & Sons Ltd., Chichester, 2009.
- [3] W. Vielstich, A. Lamm, H.A. Gasteiger, Handbook of Fuel Cells, Wiley, Chichester, 2003.
- [4] M. Carmo, D.L. Fritz, J. Mergel, D. Stolten, Int. J. Hydrogen Energy 38 (2013) 4901–4934.
- [5] E. Guilminot, A. Corcella, F. Charlot, F. Maillard, M. Chatenet, J. Electrochem. Soc. 154 (2007) B96–B105.
- [6] E. Guilminot, A. Corcella, M. Chatenet, F. Maillard, F. Charlot, G. Berthome, C. Iojoiu, J.-Y. Sanchez, E. Rossinot, E. Claude, J. Electrochem. Soc. 154 (2007) B1106–B1114.
- [7] H.A. Gasteiger, S.S. Kocha, B. Sompalli, F.T. Wagner, Appl. Catal. B: Environ. 56 (2005) 9–35.
- [8] P.J. Ferreira, G.J. Ia, Y. Shao-Horn, D. Morgan, R. Makharia, S. Kocha, H.A. Gasteiger, J. Electrochem. Soc. 152 (2005) A2256–A2271.
- [9] S. Koh, P. Strasser, J. Electrochem. Soc. 157 (2010) B585–B591.
- [10] K.C. Neyerlin, R. Srivastava, C.F. Yu, P. Strasser, J. Power Sources 186 (2009) 261–267.
- [11] J. Greeley, I.E.L. Stephens, A.S. Bondarenko, T.P. Johansson, H.A. Hansen, T.F. Jaramillo, J. Rossmeisl, J.K. Chorkendorff, J.K. Nørskov, Nat. Chem. 1 (2009) 552–556.
- [12] V.R. Stamenkovic, B. Fowler, B.S. Mun, G.F. Wang, P.N. Ross, C.A. Lucas, N.M. Markovic, Science 315 (2007) 493–497.
- [13] O. Antoine, Y. Bultel, R. Durand, P. Ozil, Electrochim. Acta 43 (1998) 3681–3691.
- [14] K. Kinoshita, J. Electrochem. Soc. 137 (1990) 845–848.
- [15] Y. Takasu, N. Ohashi, X.G. Zhang, Y. Murakami, H. Minagawa, S. Sato, K. Yahikozawa, Electrochim. Acta 41 (1996) 2595–2600.
- [16] V.R. Stamenkovic, B.S. Mun, M. Arenz, K.J.J. Mayrhofer, C.A. Lucas, G.F. Wang, P.N. Ross, N.M. Markovic, Nat. Mater. 6 (2007) 241–247.
- [17] F.J. Perez-Alonso, D.N. McCarthy, A. Nierhoff, P. Hernandez-Fernandez, C. Strebel, I.E.L. Stephens, J.H. Nielsen, I. Chorkendorff, Angew. Chem. Int. Ed. 51 (2012) 4641–4643.
- [18] L. Dubau, F. Maillard, M. Chatenet, L. Guetaz, J. Andre, E. Rossinot, J. Electrochem. Soc. 157 (2010) B1887–B1895.
- [19] F. Maillard, L. Dubau, J. Durst, M. Chatenet, J. André, E. Rossinot, Electrochem. Commun. 12 (2010) 1161–1164.
- [20] C. Cui, L. Gan, M. Heggen, S. Rudi, P. Strasser, Nat. Mater. 12 (2013) 765–771.
- [21] M. Lopez-Haro, L. Dubau, L. Guétaz, P. Bayle-Guillemaud, M. Chatenet, J. André, N. Caqué, E. Rossinot, F. Maillard, Appl. Catal. B: Environ. 152–153 (2014) 300–308.
- [22] L. Dubau, L. Castanheira, F. Maillard, M. Chatenet, O. Lottin, G. Maranzana, J. Dillet, A. Lamibrac, J.-C. Perrin, E. Moukheiber, A. Elkaddouri, G. De Moor, C. Bas, L. Flandin, N. Caqué, WIREs Energy Environ. 3 (2014) 540–560.
- [23] L. Dubau, L. Castanheira, F. Maillard, M. Chatenet, O. Lottin, G. Maranzana, J. Dillet, A. Elkaddouri, S. Basu, G. De Moor, L. Flandin, N. Caqué, Int. J. Hydrogen Energy 39 (2014) 21902–21914.
- [24] L. Castanheira, L. Dubau, M. Mermoux, G. Berthomé, N. Caqué, E. Rossinot, M. Chatenet, F. Maillard, ACS Catal. 4 (2014) 2258–2267.
- [25] J. Durst, A. Lamibrac, F. Charlot, J. Dillet, L.F. Castanheira, G. Maranzana, L. Dubau, F. Maillard, M. Chatenet, O. Lottin, Appl. Catal. B: Environ. 138–139 (2013) 416–426.
- [26] L. Dubau, M. Lopez-Haro, L. Castanheira, J. Durst, M. Chatenet, P. Bayle-Guillemaud, L. Guétaz, N. Caqué, E. Rossinot, F. Maillard, Appl. Catal. B: Environ. 142–143 (2013) 801–808.
- [27] J. Durst, M. Chatenet, F. Maillard, Phys. Chem. Chem. Phys. 14 (2012) 13000–13009.
- [28] L. Dubau, J. Durst, F. Maillard, M. Chatenet, L. Guétaz, J. André, E. Rossinot, Fuel Cells 12 (2012) 188–198.
- [29] L. Dubau, J. Durst, F. Maillard, L. Guétaz, M. Chatenet, J. André, E. Rossinot, Electrochim. Acta 56 (2011) 10658–10667.
- [30] L. Dubau, F. Maillard, M. Chatenet, J. André, E. Rossinot, Electrochim. Acta 56 (2010) 776–783.
- [31] F. Nikkuni, E. Ticianelli, L. Dubau, M. Chatenet, Electroanalysis 4 (2013) 104–116.
- [32] H.R. Colon-Mercado, H. Kim, B.N. Popov, Electrochem. Commun. 6 (2004) 795–799.
- [33] H.R. Colon-Mercado, B.N. Popov, J. Power Sources 155 (2006) 253–263.
- [34] S.C. Zignani, E. Antolini, E.R. Gonzalez, J. Power Sources 182 (2008) 83–90.
- [35] K. Schlögl, M. Hanzlik, M. Arenz, J. Electrochem. Soc. 159 (2012) B677–B682.
- [36] K. Hartl, M. Hanzlik, M. Arenz, Energy Environ. Sci. 4 (2011) 234–238.
- [37] K.J.J. Mayrhofer, S.J. Ashton, J.C. Meier, G.K.H. Wiberg, M. Hanzlik, M. Arenz, J. Power Sources 185 (2008) 734–739.
- [38] Z. Siroma, M. Tanaka, K. Yasuda, K. Tanimoto, M. Inaba, A. Tasaka, Electrochemistry 75 (2007) 258–260.
- [39] N. Takeuchi, T.F. Fuller, in: K. Fuller, V. Shinohara, P. Ramani, H. Shirvanian, S. Uchida, M. Cleghorn, S. Inaba, P. Mitsushima, H. Strasser, H.A. Nakagawa, T. Gasteiger (Eds.), Proton Exchange Membrane Fuel Cells 8, Pts 1 and 2, Electrochemical Society Inc., Pennington, 2008, pp. 1563–1571.
- [40] J. Xie, D.L. Wood, D.M. Wayne, T.A. Zawodzinski, P. Atanasov, R.L. Borup, J. Electrochem. Soc. 152 (2005) A104–A113.
- [41] F.R. Nikkuni, B. Vion-Dury, L. Dubau, F. Maillard, E.A. Ticianelli, M. Chatenet, Appl. Catal. B: Environ. 156–157 (2014) 301–306.
- [42] K.J.J. Mayrhofer, M. Hanzlik, M. Arenz, Electrochim. Acta 54 (2009) 5018–5022.
- [43] K. Schlögl, K.J.J. Mayrhofer, M. Hanzlik, M. Arenz, J. Electroanal. Chem. 662 (2011) 355–360.
- [44] A. Zana, J. Speder, M. Roefzaad, L. Altmann, M. Baumer, M. Arenz, J. Electrochem. Soc. 160 (2013) F608–F615.
- [45] J.C. Meier, I. Katsounaros, C. Galeano, H.J. Bongard, A.A. Topalov, A. Kostka, A. Karschin, F. Schüth, K.J.J. Mayrhofer, Energy Environ. Sci. 5 (2012) 9319–9330.
- [46] B. Vion-Dury, M. Chatenet, V. Vivier, Presentation of an Electrochemical Dry Cell Based on Nafion for Kinetic Studies of Pt/C Nanoparticles for PEMFC, in: 220th ECS Meeting of the Electrochemical Society, The Electrochemical Society, Boston, 2011.

- [47] F. Maillard, M. Eikerling, O.V. Cherstiouk, S. Schreier, E. Savinova, U. Stimming, *Faraday Discuss.* 125 (2004) 357–377.
- [48] M. Chatenet, L. Dubau, N. Job, F. Maillard, *Catal. Today* 156 (2010) 76–86.
- [49] H. Xu, E.L. Brosha, F.H. Garzon, F. Uribe, M. Wilson, B. Pivovar, *ECS Trans.* 11 (2007) 383–391.
- [50] Z. Xia, Q. Wang, M. Eikerling, Z. Liu, *Can. J. Chem.* 86 (2008) 657–667.
- [51] S.J. Ashton, M. Arenz, J. Power Sources 217 (2012) 392–399.
- [52] B. Vion-Dury, M. Chatenet, L. Guétaz, F. Maillard, *ECS Trans.* 41 (2011) 697–708.
- [53] L. Dubau, L. Castanheira, G. Berthomé, F. Maillard, *Electrochim. Acta* 110 (2013) 273–281.